The Effects of Varying the Combustor-Turbine Gap

N. D. Cardwell

N. Sundaram

Mechanical Engineering Department,
Virginia Polytechnic Institute and
State University,
Blacksburg, VA 24061

K. A. Thole

Mechanical and Nuclear Engineering Department,
Pennsylvania State University,
University Park, PA 16802

To protect hot turbine components, cooler air is bled from the high pressure section of the compressor and routed around the combustor where it is then injected through the turbine surfaces. Some of this high pressure air also leaks through the mating gaps formed between assembled turbine components where these components experience expansions and contractions as the turbine goes through operational cycles. This study presents endwall adiabatic effectiveness levels measured using a scaled up, two-passage turbine vane cascade. The focus of this study is evaluating the effects of thermal expansion and contraction for the combustor-turbine interface. Increasing the mass flow rate for the slot leakage between the combustor and turbine showed increased local adiabatic effectiveness levels while increasing the momentum flux ratio for the slot leakage dictated the coverage area for the cooling. With the mass flow held constant, decreasing the combustor-turbine interface width caused an increase in uniformity of coolant exiting the slot, particularly across the pressure side endwall surface. Increasing the width of the interface had the opposite effect thereby reducing coolant coverage on the endwall surface. [DOI: 10.1115/1.2720497]

Introduction

Core flow temperatures within the hot section of a gas turbine commonly exceed the metal melting temperature. Cooling techniques are needed to protect turbine components from the harsh environment. To accomplish this cooling, high pressure air is bled from the compressor, bypassed around the combustor, and then routed into the turbine where it is used for internal and external cooling purposes.

Since the entire turbine is not manufactured as a single component, numerous gaps exist between mating parts allowing leakage of high pressure coolant. Thermal expansion and mechanical stresses within the turbine make it especially difficult to seal these interfaces. One such interface is the slot between the combustor and the first stage of the turbine since the combustor and turbine are not rigidly connected. The gap between adjacent vane sections is another area that allows leakage of high pressure coolant. Leakages result in a significant loss in overall efficiency.

Turbine components are typically cast with high nickel super alloys because of their high strength at elevated temperatures. While the exact materials are proprietary, these alloys are similar in composition to Inconel 625. The average coefficient of thermal expansion for Inconel 625 is equal to 0.138 mm per cm of unrestrained metal over the standard to operating temperature range of 1075°C [1]. If one considers an unrestrained 30 cm combustor, it would result in an expansion of 4 mm. This 4 mm is on the order of the change in slot width we are modeling for this paper.

The work presented in this paper evaluates the effects of expansion and contraction of the combustor-turbine interface on endwall cooling performance. Also compared in this paper is the effect of leakage flowrates from a mid-passage gap between two mating vanes on the overall endwall cooling performance.

Relevant Past Studies

Significant work has been performed documenting the effects of leakage from the slot at the combustor-turbine interface. There have also been studies in the literature analyzing the combined effects of a combustor-turbine slot leakage and film-cooling. Very few studies exist on either the effect of a realistic mid-passage gap or the effect of changes in the combustor-turbine slot width on endwall cooling effectiveness for an actual airfoil passage.

The majority of the studies concerned with leakage flow have focused on a slot upstream of the first stage vane meant to simulate the leakage flow that occurs between the combustor and the turbine. One of the earliest works was presented by Blair [2]. Blair's study included a two-dimensional slot upstream of the vane. An enhanced cooling benefit was observed for increases in leakage flow. In a similar study, Burd et al. [3] studied the effects of coolant leaking from an upstream slot. As with Blair, Burd et al. reported better endwall cooling for leakage flows as high as 6% of the total passage flow. Colban et al. [4,5] studied the effects of changing the combustor liner film-cooling and upstream slot leakage flows on endwall effectiveness levels for a first vane cascade. Their results, like others, showed that the upstream slot flow does not evenly distribute along the endwall, with the majority of the cooling benefit along the suction side of the vane. Pasinato et al. [6] studied the effects of injecting air upstream of the vane stagnation through a series of discrete slots. These slots were oriented in the slot in such a manner that the coolant was injected tangentially to the leading edge of their contoured endwall. Pasinato et al. [6] found that this secondary air injection strongly distorted the flowfield upstream of the vane stagnation.

Some studies have combined the effects of upstream slot leakage with endwall film-cooling. The main studies performed are those of Zhang and Jaiswal [7], Kost and Nicklas [8], Nicklas [9], and Knost and Thole [10,11]. Kost and Nicklas [8] and Nicklas [9] reported that coolant ejection from an upstream slot causes radical changes in the near wall flowfield signifying an intensification of the horseshoe vortex, which was observable in their flow angle diagrams. This increase in intensity resulted in the slot coolant being moved off of the endwall surface and heat transfer coefficients that were over three times that measured for no slot flow injection. Endwall studies by Knost and Thole [10,11] investigated endwall effectiveness levels for a vane passage with both film-cooling and upstream slot injection. For increasing slot mass flow, Knost and Thole reported higher local effectiveness levels with the same coolant coverage area on the endwall

Several studies have documented the effect of flow from a gap between two adjacent airfoils. Aunapu et al. [12] showed that blowing through a passage gap could be used to reduce the negative effects of the passage vortex, but with significant aerody-

Contributed by the International Gas Turbine Institute of ASME for publication in the JOURNAL OF TURBOMACHINERY. Manuscript received July 18, 2006; final manuscript received July 26, 2006. Review conducted by David Wisler. Paper presented at the ASME Turbo Expo 2006: Land, Sea and Air (GT2006), May 8–11, 2006, Barcelona, Spain. Paper No. GT2006-90089.

namic losses. Another study done by Ranson and Thole [13] used a mid-passage gap between two blades for their experimental and computational studies. Their results showed that the flow through the gap was initially directed toward the blade pressure side, due to the incoming velocity vectors, and then convected towards the suction side of the adjacent airfoil. Yamao et al. [14] reported changes in film-cooling effectiveness levels due to leakage air injected from both an upstream slot and mid-passage gap. Their study indicated that film-cooling effectiveness was enhanced with an increase in sealing flow through both leakage interfaces.

Piggush and Simon [15,16] analyzed the effect of leakage flows on aerodynamic losses for a vane cascade. It was concluded that the mid-passage gap blowing caused both an increase in passage losses and the creation of a second smaller passage vortex which was located below the primary passage vortex. Piggush and Simon [15,16] also concluded that the majority of mid-passage gap blowing became entrained in the formation of a second vortex within the passage. Reid et al. [17] studied the effect of interplatform leakage on overall efficiency for an axial flow turbine stage. They determined that the largest drop in efficiency associated with interplatform leakage was 1.5% when compared to the stage efficiency with no slot present. The main difference in interplatform gap geometry between these two studies is that Reid et al. [17] modeled the internal seal strip of the interplatform gap and Piggush and Simon [15,16] did not.

Cardwell et al. [18] analyzed the effect of a mid-passage gap with a seal strip and platform misalignment on endwall cooling effectiveness. They determined that misalignment between adjacent vanes and between the combustor-turbine interface can significantly affect upstream slot coolant trajectory and effectiveness. Cardwell et al. [18] reported that a backward facing step (cascade configuration) between the combustor-turbine interface greatly reduced the need for suction side endwall film-cooling due to an increased utilization of upstream slot leakage.

The effect of a step in hub diameter just ahead of a blade row on aerodynamic blade performance was evaluated by de la Rosa Blanco et al. [19]. They also determined that a backward facing step at this location can lead to a reduction in endwall and mixing losses when compared to a flat endwall while a forward facing step produces higher losses than a flat endwall. Piggush and Simon [15,16] also agreed with the pressure loss results of de la Rosa Blanco et al. [19] for a turbine vane indicating increased losses with a forward and decreased losses with a backward facing step upstream of the vane stagnation.

To date there has been significant research on the effect of upstream slot flow on the passage fluid dynamics and endwall heat transfer, but no study on the effects of varied upstream slot widths. This study improves upon previous works by studying the realistic effect of combustor-turbine slot expansion and contraction on endwall adiabatic effectiveness levels given a vane passage with other realistic features such as a mid-passage gap and film-cooling.

Vane and Endwall Geometry

The flat endwall used in the linear cascade has three cooling features: a combustor-turbine slot, a mid-passage vane-to-vane gap with accompanying seal strip, and discrete film cooling holes. The same film cooling pattern as shown in Fig. 1, which was originally designed and tested by Knost and Thole [10,11], was used in this study. Figure 1 shows the film cooling hole injection angles, the upstream slot, and the mid-passage gap discussed above. All film cooling holes were cylindrical and inclined at an angle of 30 deg with respect to the endwall surface. Table 1 provides a brief description of the turbine vane geometry and operating conditions. Significant studies were performed on this particular vane geometry with a more detailed description given in Radomsky and Thole [20].

Figure 1 also shows a two-dimensional slot upstream of the vane leading edge, which represents the mating interface of the turbine and combustor. This slot had an injection angle of 45 deg and was located 30% of the axial chord upstream of the vane stagnation location. This leakage interface will be referred to as the upstream slot. Table 2 provides a summary of parameters relevant to the film-cooling holes and upstream slot geometries.

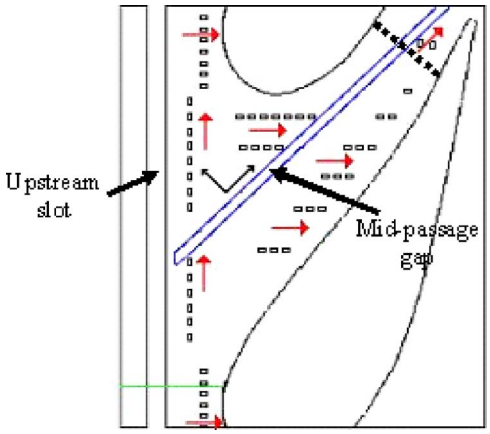

Fig. 1 Endwall geometry with film-cooling holes, an upstream slot, and a mid-passage gap

As discussed in the Introduction, the primary focus of this work was to analyze the endwall cooling effect of upstream slot expansion and contraction. For this study the metering slot width was expanded by 50% and contracted by 50%, which will be referred to as double width and half width, respectively. As with the nominal slot, both the double width and half width slots had a 45 deg surface injection angle. For these studies, the upstream slot was expanded and contracted while keeping the slot centerline fixed relative to the vane stagnation.

The gap between adjacent vane sections will be referred to as the mid-passage gap. A cross section of the mid-passage gap is shown in Fig. 2. Unlike the upstream slot, the mid-passage gap had a recessed seal strip as found in many engine designs, which influenced its interaction with the coolant and mainstream flow. To allow flow control, the mid-passage gap had a separate supply plenum which did not open into the upstream slot. The cross section of the mid-passage gap is also shown in Fig. 2. This gap, which was described in the previous study by Cardwell et al. [18],

Table 1 Geometric and flow conditions

Scaling factor	9
Scaled up chord length (C)	59.4 cm
Scaled up axial chord length (C_a)	29.3 cm
Pitch/chord (P/C)	0.77
Span/chord (S/C)	0.93
Re_{in}	2.1×10^5
Inlet and exit angles	0 to 72 deg
Inlet, exit Mach number	0.017, 0.085
Inlet mainstream velocity	6.3 m/s

Table 2 Summary of endwall geometry

	Parameter	Experimental
Upstream slot	Nominal slot width	0.024 C
	Double slot flow length to width	0.94
	Nominal slot flow length to width	1.9
	Half slot flow length to width	3.8
	Upstream slot surface angle	45 deg
Film cooling	FC hole diameter (cm)	0.46
	FC hole L/D	8.3
	Film-cooling surface angle	30 deg

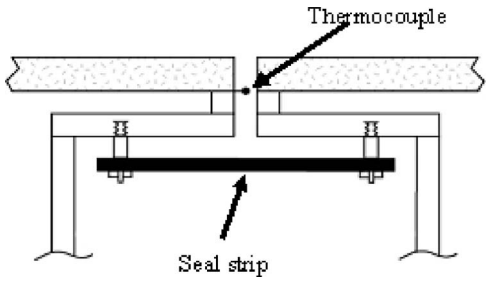

Fig. 2 Cross section view of the mid-passage gap geometry with an accompanying seal strip

had a 90 deg surface injection angle, a width of 0.635 cm, and a gap flow length to width ratio of 5. For this study, the mid-passage gap width was not varied.

Similar to the previous study reported by Cardwell et al. [18], the endwall surface was covered with a uniform roughness. To simulate a random array of a uniform roughness level, wide-belt industrial sandpaper was used to cover the entire endwall. The sandpaper had a closed coat 36 grit surface and a grade Y cloth backing. A closed coat surface had roughness elements arranged in a random array over 100% of its surface. The 36 grit sandpaper had an average particle size of 538 microns [21] which was roughly twice that observed by Bons et al. [22] for in service turbine endwalls. A custom construction technique was used to guarantee a uniform and uniform fit around each film-cooling hole. This technique ensured a uniform interaction between the rough surface and coolant jets for the entire endwall.

Experimental Methodology

The experimental facility used for this study consisted of a linear cascade test section placed in a closed loop wind tunnel, as shown in Fig. 3. Flow within the wind tunnel was driven by a 50 hp axial vane fan, which was controlled by a variable frequency inverter. After being accelerated by the fan, the flow turned 90 deg and then passed through a primary finned-tube heat exchanger. This heat exchanger was used to precool the bulk flow. After passing through the primary heat exchanger, the flow encountered another 90 deg turn before entering a three way split. This split simulated the primary core flow through the combustor and the bypass flow around the combustor. The flow split was achieved by using a porous plate with a 25% open area to act as a valve thereby directing a portion of the flow into the upper channel. The primary core flow passed through a resistance heater bank where its temperature was increased to 60°C. The secondary flow in the top channel passed through a secondary finned-tube heat exchanger where the flow temperature was lowered to 10°C. The mainstream flow continued through the middle channel into the test section. The cooler bypass flow was pulled into a 2 HP blower where it then flowed into the test section for the coolant supplies.

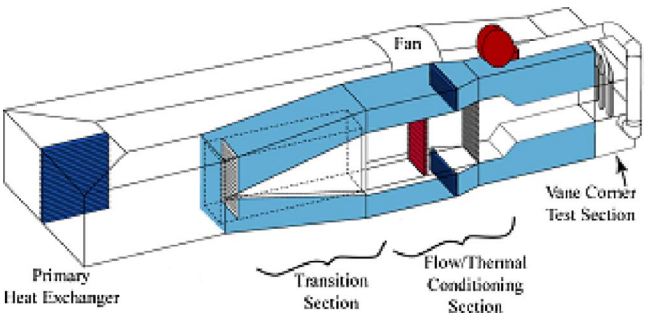

Fig. 3 Illustration of the wind tunnel facility

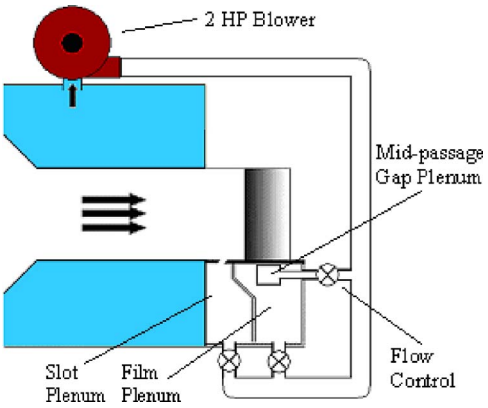

Fig. 4 Separate plenums for film-cooling, upstream slot, and mid-passage gap provided by independent flow control

The test section consisted of a vane cascade comprised of two full passages with one center vane and two half vanes, an endwall with film cooling holes, an upstream slot, and mid-passage gap geometries, which were scaled up by a factor of 9. A detailed account of its construction has been previously described by Cardwell et al. [18]. The two main differences between the current test section and the one described by Cardwell et al. [18] were a change in the upstream approach flow and the ability to vary the upstream slot metering width. The previous upstream approach flow had a 15.6 deg contraction directly upstream of the test section while the upstream flow path used in this study had a 45 deg contraction that was 2.9 chords upstream of the vane giving a longer constant flow area into the test section. The upstream slot was interchangeable so that the flow metering width could be adjusted. The endwall, which was the main focus of the study, was constructed of low thermal conductivity foam (0.033 W/m K). The endwall foam was 1.9 cm thick and was mounted on a 1.2 cm thick Lexan plate. The cooling hole pattern was cut using a five-axis water jet machine to ensure proper hole placement and tight dimensional tolerances. The upstream slot, which needed to be stiffer, was constructed of hard wood which also has a low thermal conductivity value (0.16 W/m K).

Adiabatic endwall temperatures were taken for the different slot geometries and flowrates and also for different gap flowrates. Each coolant path had its own separate plenum for independent control of the flow through the film-cooling holes, upstream slot, and mid-passage gap as shown in Fig. 4. For the studies reported in this paper, film cooling was not varied so a nominal value was set for all cases. The mid-passage gap was maintained even when no coolant was supplied to its plenum. Experiments were conducted for both a sealed and leaking mid-passage gap. Sealing of the mid-passage gap plenum was accomplished by closing the appropriate coolant feed pipe.

The inlet turbulence was measured to be 1.3%. The turbulent inlet boundary layer thickness was measured as 22% of the span at a location 15 slot widths upstream of the center vane stagnation location. During steady state operation, a temperature difference of 40°C was maintained between the mainstream and the coolant. From a room temperature start, the typical time to achieve steady state conditions was 3 h.

Coolant Flow Settings. As stated earlier, all three coolant plenums were sealed with respect to each other and had independent flow control. CFD studies reported by Knost and Thole [10] were used to set the coolant mass flows through the film-cooling holes through the use of a predicted discharge coefficient. The method previously described by Knost and Thole and Cardwell et al. [18] was used whereby a global discharge coefficient was found through CFD analysis. Only one film-cooling flowrate was used

for these studies, which was 0.5% of the core flow.

A discharge coefficient of 0.6 was chosen for the upstream slot. This is a typically assumed value for a flow through a sharp-edged orifice. No assumed discharge coefficient was needed for the mid-passage gap as the coolant flow rate was measured directly using a laminar flow element placed downstream of the coolant control valve. Feeding this plenum differently was necessary due to the high amounts of ingestion seen in the mid-passage gap, which will be explained later in the paper.

Instrumentation and Measurement Techniques. Spatially-resolved adiabatic endwall temperature contours were recorded using an FLIR P20 infrared camera. The test section had multiple viewing ports on the top endwall through which measurements were taken until the entire endwall surface was mapped. At each viewing location the camera was placed perpendicular to the endwall surface at a distance of 55 cm. Given the camera's viewing angle, each picture covered an area of 24 cm $\times$ 18 cm, with the resolution being 320×240 pixels. The camera's spatial integration was 0.16 hole diameters (0.71 mm). Postcalibration of the images was accomplished using actual temperature values taken by thermocouples placed on the endwall surface. The surface emissivity was assumed to be 0.92, which is a commonly reported value for the material type and surface structure associated with coarse grit sandpaper [23]. During postcalibration, the image background temperature was adjusted until the thermocouple data and infrared image data were within 0.01°C. Typical values of background temperature were 55°C (note the freestream temperature was typically 60°C). Six images were taken at each viewing location, of which five were used to obtain an average image using an in-house Matlab program. The same program then scales, rotates, and assembles the averaged images at all locations. This fully assembled contour gives a complete temperature distribution for the endwall surface.

Freestream temperature values were measured at 25%, 50%, and 75% of the vane span at four locations across the passage pitch. Maximum variations along the pitch and span were less than 0.5°C and 1.0°C, respectively. Three thermocouples were attached in the upstream slot plenum and two thermocouples were attached in the film cooling plenum to measure the respective coolant temperatures. Differences in temperature between the plenums were typically less than 1°C. Eleven thermocouples were placed within the mid-passage gap to measure the air temperature profile. These thermocouples were located six seal strip thicknesses beneath the endwall surface (see Fig. 2). A 32 channel data acquisition module by National Instruments was used with a 12-bit digitizing card to measure and record the thermocouple voltage data. All temperature data was recorded and compiled after the system had reached steady state.

A one-dimensional conduction correction as described by Ethridge et al. [24] was applied to all adiabatic effectiveness measurements. This correction involved measuring the endwall surface effectiveness with no coolant flow. This was accomplished by blocking off the film-cooling holes within the passage. The resulting η correction was 0.16 at the entrance for an η value of 0.9 and 0.02 at the exit region at a measured η value of 0.5.

An uncertainty analysis was performed on the measurements of adiabatic effectiveness using the partial derivative method described at length by Moffat [25]. The precision uncertainty was determined by taking the standard deviation of six measurement sets of IR camera images with each set consisting of five images. The precision uncertainty of the IR camera measurements was ±0.0143°C and the bias uncertainty was ±1.02°C, based on the calibration of the image. The precision uncertainty and bias uncertainty of the thermocouples was ±0.1°C and ±0.5°C, respectively. The total uncertainty was then calculated as ±1.02°C for the IR images and ±0.51°C for the thermocouples. Uncertainty in effectiveness, η, was found based on the partial derivative of η with respect to each temperature in its definition and the total uncertainty in the measurements. Uncertainties of $\delta\eta = \pm 0.028$ at $\eta = 0.1$ and $\delta\eta = \pm 0.028$ at $\eta = 0.8$ were calculated.

Table 3 Upstream slot coolant setting

	% mass flow	M	I
Double width slot	0.85%	0.22	0.04
	1.13%	0.29	0.08
Nominal slot width	0.75%	0.29	0.08
	0.85%	0.33	0.10
	1.00%	0.39	0.13
Half-width slot	0.38%	0.29	0.08
	0.85%	0.66	0.39

Discussion of Results

A number of tests were conducted for this study with the most representative results being given in this paper, as described in the next section on the test matrix. First, the effect of varying upstream slot width will be discussed for constant mass flow rate and a constant momentum flux ratio. Second, the effect of a fixed slot width for varying upstream slot mass flow rate will be discussed. Last, a mid-passage gap comparison with and without flow width will be discussed.

Derivation of Test Matrix. Significant consideration was given to the creation of a test matrix (shown in Table 3), which would be of particular use to the turbine designer. Mass flowrates are reported on a percent basis with respect to the total mass flowrate through the passage. For all cases, the film-cooling mass flow was set at 0.5% and, unless specified, the mid-passage gap was at 0%.

The first comparison done was for a 0.85% matched mass flow for expanding and contracting the slot width by 50%. The mass flow was kept constant by increasing or decreasing the plenum pressure accordingly, which resulted in a matched mass flow but varying momentum flux and mass flux ratios. While a sensible choice from an experimental point of view, this does not necessarily correlate to that of an actual engine.

Within the engine, the pressure difference between the coolant and exit static pressure typically remains constant resulting in a matched momentum flux ratio (given that $\Delta p \sim U^2$). The second comparison was for an average slot $I = 0.08$ while expanding and contracting the slot width 50%. Total coolant pressure to static gas pressure was held at a constant value, which resulted in nominally the same average slot velocity (and momentum flux ratio) but differing slot mass flows as the slot metering width was contracted or expanded. Next, the effect of varying slot mass flow was analyzed for the nominal slot width. The last effect to be analyzed was the mid-passage gap leakage. The mid-passage gap mass flow was set at 0.1%, 0.2%, and 0.3% of core passage flow.

Matched Mass Flow Ratios for Differing Slot Widths. For nominal slot flow rate of 0.85%, Fig. 5 compares adiabatic effectiveness for different slot widths. It is important to note that while the slot mass flow remained constant for all slot widths, the average slot momentum flux ratio changed by a factor of 10 between the half and double width slots.

The effect of expanding the slot is shown in Fig. 5(*a*). No coolant was observed exiting the upstream slot on the pressure side of the mid-passage gap. The hot ring observed on the vane's leading edge was apparent and effectiveness levels on the entire pressure side and suction side had decreased substantially relative to Fig. 5(*b*). The effect of contracting the slot is shown in Fig. 5(*c*). Figures 5(*a*) and 5(*b*) show the upstream slot coolant had been primarily confined to the suction side surface by the presence of the mid-passage gap. In Fig. 5(*c*) for the half width slot the leakage flow seems evenly distributed over the entire slot pitch with a substantial increase in cooling on the pressure side of the mid-passage gap. Film-cooling holes upstream of the vane stagnation are redundant and the hot ring around the vane pressure

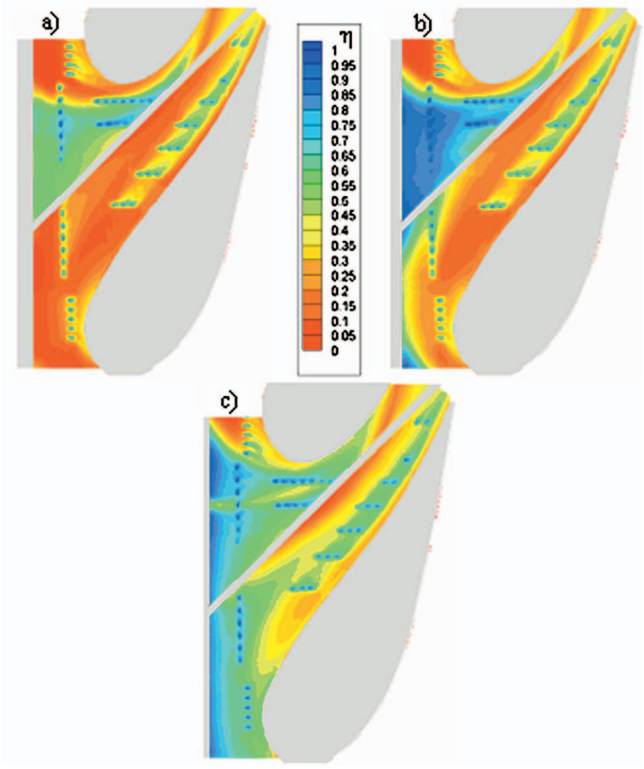

Fig. 5 Contours of adiabatic effectiveness for (*a*) double, (*b*) nominal, (*c*) half-width upstream slot with 0.85% slot mass flow ratio

side shown in other cases which extends from the leading edge into the passage is no longer apparent. More even cooling was observed on the mid-passage gap suction side as well in Fig. 5(*c*), while the locally high values of effectiveness seen using the nominal upstream slot width (Fig. 5(*b*)) were less apparent.

Pitchwise averaged values of effectiveness for varied slot width with matched mass flow ratios are shown in Fig. 6. Expanding the slot shows a decrease in averaged effectiveness levels along much of the platform while contracting the slot increases the averaged effectiveness. This can be explained by the contours shown in Fig. 5 where the coverage area was greater in Fig. 5(*c*) and more localized in Fig. 5(*a*). The contracted slot shows better coolant coverage than nominal with higher averaged effectiveness levels than both the nominal and double-width slot. This result is expected based on the viewpoints of coolant momentum and mass flow (see Table 3). The higher plenum pressure required to supply

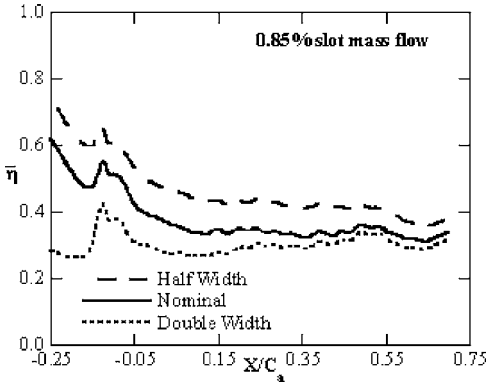

Fig. 6 Pitchwise averaged adiabatic effectiveness for the entire passage with varied upstream slot widths

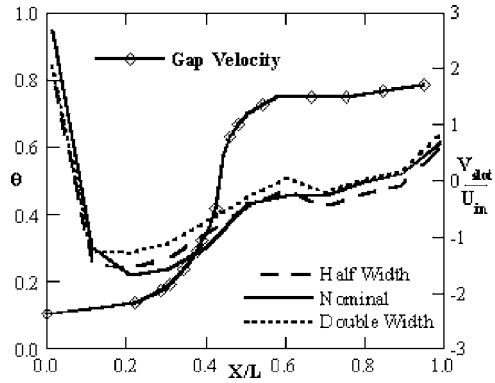

Fig. 7 Nondimensionalized mid-passage gap temperature profiles with varied upstream slot widths

0.85% from the contracted slot has resulted in an increase in the coverage uniformity. This improvement in uniformity can be explained by considering that with a higher plenum pressure there is less sensitivity to the exit static pressure variation due to the presence of the vane. For the expanded slot, lower plenum pressures are required to supply 0.85% mass flow thereby resulting in more sensitivity to the exit static pressure.

Through observation of Fig. 5(*a*) it was concluded that a portion of the slot was ingesting hot mainstream air since no coolant was observed exiting the slot on the mid-passage gap pressure side. Therefore, the ejected coolant on the suction side was already premixed with hot main gas within the upstream slot, which explains the strong reduction in averaged effectiveness levels for the expanded slot.

Mid-passage gap temperature profiles are shown in Fig. 7. This information is important as turbines are typically designed so that ingestion of hot mainstream gas into the gaps is minimized. The nondimensional gap temperature, θ, was based on the mainstream and the coolant temperatures where θ values of zero and one signify maximum and minimum gap temperatures, respectively. Again, Fig. 2 illustrates the thermocouple location for the mid-passage gap. Also shown in Fig. 7 are the calculated inviscid gap velocities based on the local static pressure at the gap exit, which was known from previous studies [26]. Note that this calculation assumed a constant total plenum pressure difference between the mainstream and the gap plenum. An iterative procedure was used to calculate the pressure difference which resulted in zero net mass flow from the slot (ingested flow equals ejected flow). For zero net mass flow through the mid-passage gap, negative velocity values (signifying ingestion) were predicted for $X/L<0.45$ and positive velocity values (signifying ejection) were predicted for $X/L>0.45$.

The gap leading edge ingested a substantial amount of coolant from the upstream slot. In the location $0<X/L<0.2$, this ingested coolant resulted in cooler temperatures with the amount of coolant being ingested decreasing with increasing X/L. There was also increased ingestion of the hot mainstream flow which caused a rapid increase in the gap air temperature. Temperature in the gap increased dramatically as hot mainstream flow was ingested at $X/L<0.2$. The increase in θ observed at $X/L=0.2$ was most likely caused by ingestion of fresh coolant from film-cooling holes in the vicinity of $X/L=0.2$ as well as continued mixing of previously ingested upstream slot coolant and main gas. This mixture of coolant and hot mainstream gas convects inside the mid-passage gap until the exit static pressure is low enough for it to exit the gap. Up to $X/L=0.45$, the inviscid velocity is indicated to be into the slot (static endwall pressure is higher than the plenum pressure), which is consistent with the fact that flow is ingesting into the gap. Beyond $X/L=0.45$, Fig. 7 shows that flow is exiting the mid-passage gap.

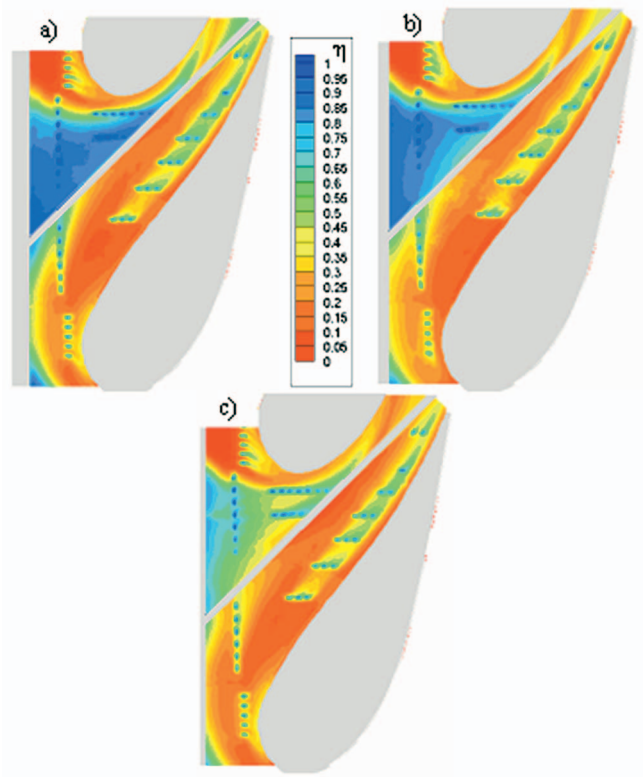

Fig. 8 Contours of adiabatic effectiveness for (*a*) double, (*b*) nominal, (*c*) half-width upstream slot with *I*=0.08 average slot momentum flux ratio

All θ profiles for varying slot width in Fig. 7 are very similar to values slightly lower for both the double and half-width upstream slots. Since the coolant exiting the half-width slot has a relatively high momentum compared with the nominal, it is less likely that it will be ingested into the mid-passage gap than for the double-width slot.

Matched Momentum Flux Ratios for Differing Slot Widths. Upstream slot momentum flux ratios were matched to an average value of $I=0.08$, which corresponded to a nominal width upstream slot flow of 0.75%. As shown previously, the upstream slot width was contracted and expanded by 50%. There was 0% flow in the mid-passage gap.

Figure 8 shows contours of adiabatic effectiveness and Fig. 9 shows pitchwise averaged values of adiabatic effectiveness on the endwall for an average upstream slot momentum flux ratio of

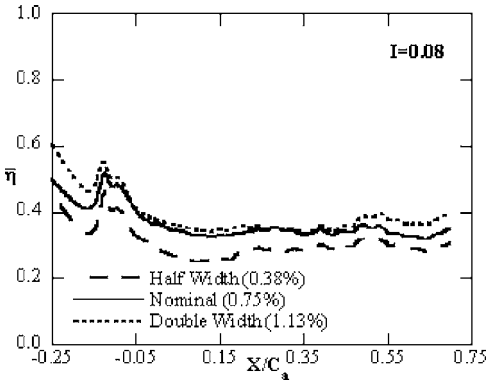

Fig. 9 Plots of pitchwise averaged adiabatic effectiveness for the entire passage with varied slot widths

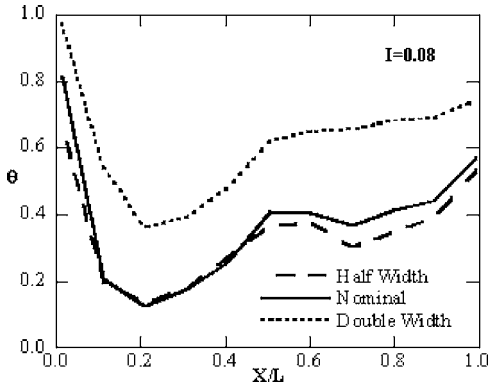

Fig. 10 Nondimensionalized mid-passage gap temperature profiles varied upstream slot widths given a nominal slot momentum flux ratio

0.08. The coolant coverage area is very similar for all three slot widths, illustrating that coverage area is a function of the coolant to mainstream momentum flux ratios rather than the coolant mass flow rate. By contracting the slot and keeping the plenum-to-mainstream pressure difference the same, the mass flow of coolant exiting the upstream slot was reduced (see Table 3). This reduction in coolant flow explains the observed reduction in effectiveness on the suction side platform and the lower values of averaged effectiveness. By the same reasoning, the coolant mass flow would be higher for the expanded slot, thus explaining the increase in averaged coolant effectiveness on the suction side platform.

Figure 8 shows there is also an effect of slot width on the mid-passage gap trailing edge. In this region, the mid-passage gap ejects a mixture of the coolant and main gas which was ingested in the leading edge region. A slight increase in effectiveness levels for the nominal and double slot cases relative to the half slot width were observed on the suction side of the mid-passage gap trailing edge. The cooler region near the trailing edge indicates different amounts of coolant were being ingested into the mid-passage gap near the leading edge and then ejected near the trailing edge. Upstream slot momentum flux was the same for all cases, but coolant mass flow was higher for the double slot and lower for the half slot.

By examining the mid-passage gap temperature profiles in Fig. 10, we see that by matching the upstream slot coolant momentum flux ratios the amount of coolant being ingested into the mid-passage gap changed with slot width. Expanding the slot width dramatically decreased gap temperature, sometimes by as much as 70% from nominal. The effect of contracting the slot is not observed until $X/L=0.45$, where ejecting mid-passage gap temperatures were observed to be 10–20% lower.

Adiabatic Effectiveness With Varying Slot Leakage Flows. For a constant upstream slot width and a varying difference between the coolant and the mainstream static pressures, the coolant flow rate exiting the slot varies. To determine this effect, tests were conducted, as before, with no mid-passage gap flow and upstream slot mass flow rates were set to 0.75%, 0.85%, and 1.0%. The effect of varying upstream slot flowrate was analyzed for a nominal slot width. Contours of adiabatic effectiveness for the effect of coolant mass flux ratio are shown in Fig. 11.

The primary result was that for all three cases the coverage area had not changed significantly but the cooling benefit had increased. It is important to note that upstream slot momentum flux ratio increased with slot mass flow by a factor of 1.6 from the lowest to highest slot flowrate studied. This increase was much smaller than the factor of 10 discussed in the previous section. For each case, there was very little coolant flow from the upstream slot crossing over the mid-passage gap as shown before by Card-

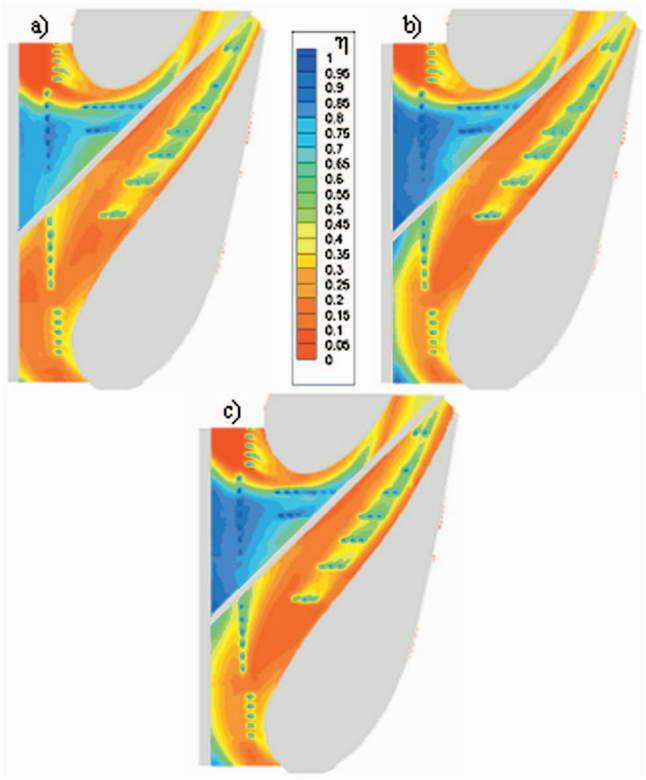

Fig. 11 Contours of adiabatic effectiveness for (*a*) 0.75%, (*b*) 0.85%, (*c*) 1.0% upstream slot mass flow rate for a nominal slot width

well et al. [18]. The coolant convected along the gap until the end of the vane passage where it exited the gap. The effect of film-cooling was also nominally the same for all upstream slot flows. As the slot mass flow rate was increased, the amount of coolant observed on the pressure side of the slot increased slightly. The suction side of the gap, which was well cooled for all flow rates, showed higher adiabatic effectiveness levels when the slot flow rate was increased. Although the coolant mass flow rate through the slot was increased substantially, much of the pressure side endwall continued to show lower values of adiabatic effectiveness. To quantify the effect of increasing slot flow at these levels, the adiabatic effectiveness values were pitchwise averaged for all flow rates, as shown in Fig. 12. Increasing the upstream slot cooling showed increased values of pitchwise averaged adiabatic

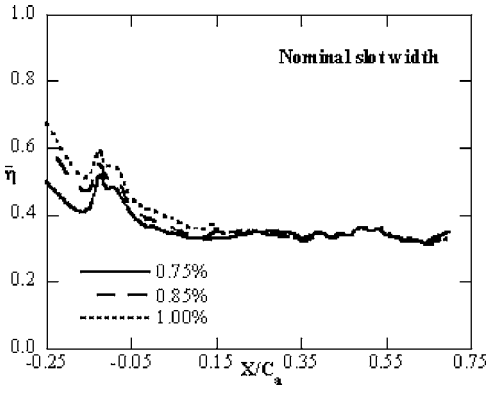

Fig. 12 Plots of laterally averaged adiabatic effectiveness for the entire passage with varied upstream slot mass flow

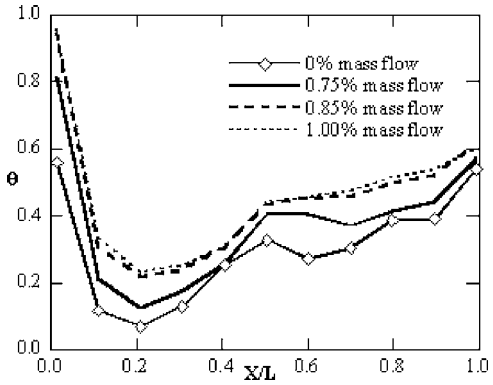

Fig. 13 Nondimensionalized mid-passage gap temperature profiles varied upstream slot mass flow

effectiveness.

Since there was more coolant on the endwall for increased upstream slot leakage, it was hypothesized that more coolant was being ingested into the mid-passage gap. The measured nondimensional gap temperature profiles for the above mentioned cases are shown in Fig. 13. Note that again, no coolant mass flow was provided to the gap. The increase in slot flow rate from 0.75% to 0.85% showed a substantial decrease in gap temperatures. The ratio of ingested coolant to hot gas was higher, thus explaining the decrease in ejected gap temperatures beyond $X/L=0.45$. In contrast, negligible changes in gap temperatures were recorded for the increase to 1% upstream slot flow. Most likely the gap was saturated with coolant from the upstream slot at the 1% case.

Adiabatic Effectiveness Varying Mid-Passage Gap Flows. The last comparison completed for this study was for a variation in the mid-passage gap leakage. These experiments were conducted with a nominal upstream slot width and a 0.75% upstream slot mass flow rate ($I=0.08$). Mid-passage gap mass flow rates were set to 0.1%, 0.2%, and 0.3%.

The contours of adiabatic effectiveness for the varying gap flows are shown in Fig. 14. These contours are very similar to each other with no large effect due to varied mid-passage gap flow. As before, the contours were pitchwise averaged, which is shown in Fig. 15. No effect is observed in the leading edge region of the slot. It appears that the mid-passage gap flow has little to no effect on the endwall surface for the entire passage in this flow rate range. The presence of the gap, however, does affect the endwall effectiveness patterns relative to a continuous endwall as previously described by Cardwell et al. [18].

There was a slight effect of the coolant flow rate on the nondimensional temperature distribution within the gap. Figure 16 shows the nondimensional gap temperature profiles for the three cases as compared to the no flow case. As compared to the no gap flow condition, the gap temperature was lower relative to all values of coolant mass flow. Increasing the mid-passage gap flow rate reduced the temperature measured within the gap for $0.45<X/L<1$. For between $0.45<X/L<1$, decreases in gap temperatures were observed for increases in mid-passage gap flow. Note that the ejected fluid was a mixture of ingested upstream slot coolant, ingested main gas, and mid-passage gap coolant.

Figure 17 shows thermal field profiles which were taken within the passage for 0% and 0.3% mid-passage gap flow. The measurement plane was located at $s/C=0.5$, which is illustrated by the dashed line in Fig. 1. There was little change in the passage temperature profiles indicating little change in the secondary flows. Again as previously noted when comparing gap temperature profiles, the interaction of the mid-passage gap was only slightly affected by changes in leakage flow and was primarily driven by the endwall static pressure distribution throughout the passage.

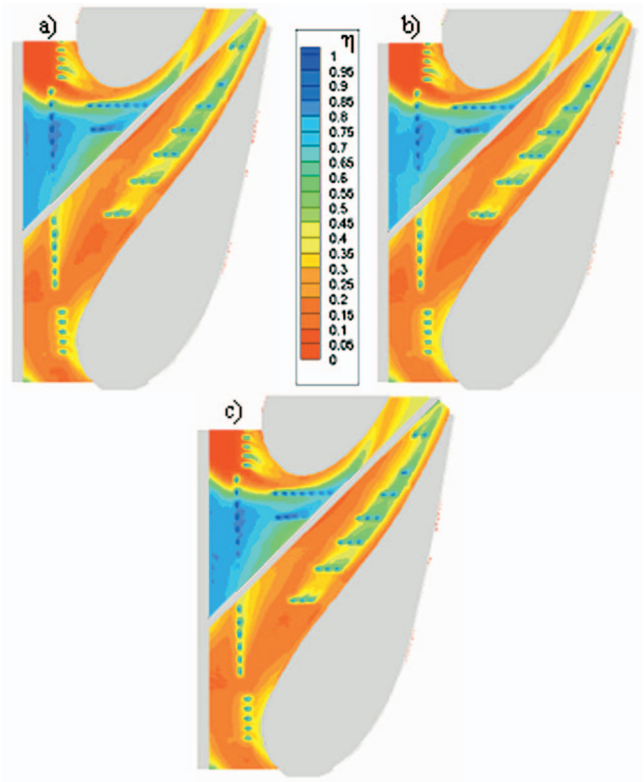

Fig. 14 Contours of adiabatic effectiveness for (*a*) 0.1%, (*b*) 0.2%, and (*c*) 0.3% mid-passage gap mass flow with nominal upstream slot width

Conclusions

Measurements of endwall adiabatic effectiveness and nondimensional mid-passage gap temperature profiles were presented for a double, nominal, and half-width combustor to turbine interface. Two parameters were used to compare the different configurations: mass flow and momentum flux ratios.

When comparing varying slot width while matching mass flow, it was observed that decreasing the slot width caused the coolant to be more evenly distributed on the endwall. Increasing the slot width while matching mass flow indicated a reduced coverage with no coolant observed on the pressure side of the passage. Moreover, the effectiveness values on the suction side were lower that those observed at the same flow rate for a nominal slot width. This decrease was caused by ingesting hot mainstream gas. Averaged effectiveness values were found to be the lowest for the double slot relative to the nominal and half-width.

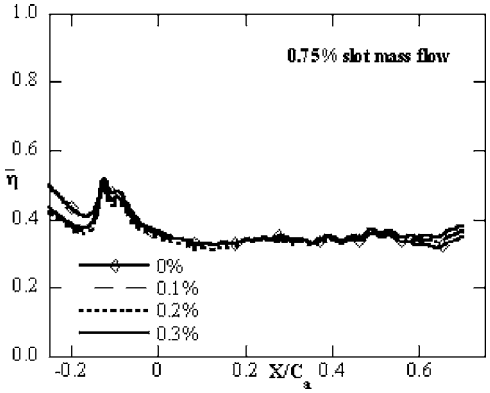

Fig. 15 Plots of laterally averaged adiabatic effectiveness for the entire passage with varied mid-passage gap cooling

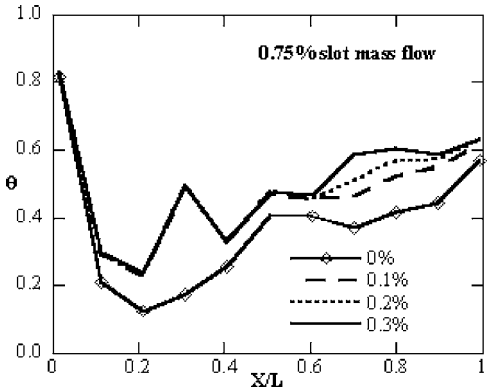

Fig. 16 Nondimensionalized mid-passage gap temperature profiles with varied mid-passage gap cooling

Matching the slot momentum flux ratios for the three slot widths resulted in endwall contours that looked nominally the same in terms of upstream slot coolant coverage. These results indicated that the upstream coolant coverage area was a function of momentum flux ratio, not mass flow rate. The cooling from the upstream slot had a beneficial effect only along the suction side endwall surface. Doubling the slot width resulted in better endwall cooling on the suction side platform and significantly lowered temperatures within the mid-passage gap. Given the same slot momentum flux ratio, halving the slot resulted in less coolant mass flow and higher temperatures within the gap.

With a nominal width, increasing upstream slot cooling resulted in improved endwall adiabatic effectiveness values and lower gap temperatures. Even at 1.0% mass flow, the upstream coolant momentum was still too low to adequately cool the pressure side platform due to the presence of the ingesting mid-passage gap.

Mid-passage gap leakage flows proved to have little effect on endwall adiabatic effectiveness levels, though gap temperatures were lower for increased leakage flows. Since the gap plenum was ingesting, it was at an equilibrium pressure somewhere between the passage inlet static wall pressure, which was higher, and the passage exit static wall pressure, which was lower. By introducing coolant flow to the gap plenum, the temperature of the gap fluid was effectively lowered while the equilibrium pressure stayed nominally the same. Thus it would require much higher coolant pressure to significantly affect the mid-passage gap velocity distribution.

These results indicate that the leakage through the combustor-turbine interface can provide cooling to the endwall. Since this interface width changes as the turbine and combustor heat up, it is important to account for the associated changes in coolant cover-

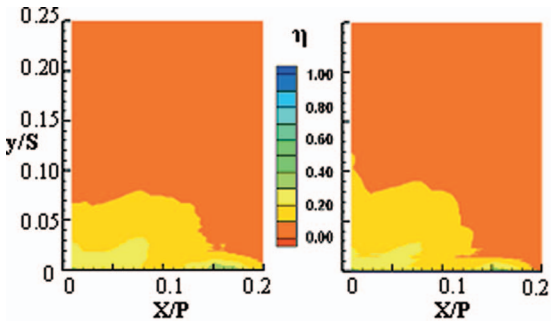

Fig. 17 Plots of thermal field data for (*a*) 0% flow and (*b*) 0.3% flow within the mid-passage gap

age area and local coolant levels thereby reducing the need for film-cooling on certain areas of the vane-endwall surface.

Acknowledgment

This publication was prepared with the support of the U.S. Department of Energy, Office of Fossil Fuel, and National Energy Technology Laboratory and the South Carolina Institute for Energy Studies (SCIES) University Turbine Systems Research program (UTSR). However, any opinions, findings, conclusions, or recommendations expressed herein are solely those of the authors and do not necessarily reflect the views of the DOE, SCIES, or the UTSR Program. The authors would also like to thank Mike Blair (Pratt & Whitney), Ron Bunker (General Electric), and John Weaver (Rolls Royce) for their input on the modeling of realistic turbine features.

Nomenclature

C = true chord of stator vane
C_a = axial chord of stator vane
D = diameter of film-cooling hole
I = average momentum flux ratio, $I=(\rho_c U_c^2/\rho_\infty U_\infty^2)$ $=\rho_s(\dot{m}/\rho_s A_s)^2/\rho_\infty U_\infty^2$
L = length of mid-passage gap
$\dot{m}$ = mass flowrate
M = average blowing ratio
p = static pressure
P = vane pitch, hole pitch
Re_{in} = Reynolds number, $\mathrm{Re}_{in}=\mathrm{CU}_{in}/\nu$
S = span of stator vane
T = temperature
X = local coordinate
U = velocity
s = distance along vane from flow stagnation

Greek

η = adiabatic effectiveness, $\eta=(T_\infty-T_{aw})/(T_\infty-T_c)$
ρ = density
ν = kinematic viscosity
θ = nondimensional gap effectiveness, $\theta=(T_\infty-T_G)/(T_\infty-T_c)$

Subscripts

aw = adiabatic wall
c = coolant conditions
G = gap air temperature
in = inlet conditions
s = upstream slot
∞ = freestream conditions

References

[1] Electronic Space Products International "Inconel 625," http://www.espimetals.com/tech/Tech%20Inconel%20625.htm (Ashland, OR).
[2] Blair, M. F., 1974, "An Experimental Study of Heat Transfer and Film-Cooling on Large-Scale Turbine Endwall," ASME J. Heat Transfer, **96**, pp. 524–529.
[3] Burd, S. W., Satterness, C. J., and Simon, T. W., 2000, "Effects of Slot Bleed Injection Over a Contoured Endwall on Nozzle Guide Vane Cooling Performance: Part II—Thermal Measurements," ASME Paper No. 2000-GT-200.
[4] Colban, W. F., Thole, K. A., and Zess, G., 2002, "Combustor-Turbine Interface Studies: Part 1: Endwall Measurements," J. Turbomach., **125**, pp. 193–202.
[5] Colban, W. F., Lethander, A. T., Thole, K. A., and Zess, G., 2002, "Combustor-Turbine Interface Studies: Part 2: Flow and Thermal Field Measurements," J. Turbomach., **125**, pp. 203–209.
[6] Pasinato, H. D., Squires, K. D., and Roy, R. P., 2004, "Measurement and Modeling of the Flow and Heat Transfer in a Contoured Vane-Endwall Passage," Int. J. Heat Mass Transfer, **47**, pp. 5685–5702.
[7] Zhang, L. J., and Jaiswal, R. S., 2001, "Turbine Nozzle Endwall Film-Cooling Study Using Pressure Sensitive Paint," J. Turbomach., **123**, pp. 730–738.
[8] Kost, F., and Nicklas, M., 2001, "Film-Cooled Turbine Endwall in a Transonic Flow Field: Part I—Aerodynamic Measurements," ASME Paper No. 2001-GT-0145.
[9] Nicklas, M., 2001, "Film-Cooled Turbine Endwall in a Transonic Flow Field: Part II—Heat Transfer and Film-Cooling Effectiveness," J. Turbomach., **123**, pp. 720–729.
[10] Knost, D. G., and Thole, K. A., 2003, "Computational Predictions of Endwall Film-Cooling for a First Stage Vane," ASME Paper No. GT2003-38252.
[11] Knost, D. G., and Thole, K. A., 2005, "Adiabatic Effectiveness Measurements of Endwall Film-Cooling for a First Stage Vane," J. Turbomach., **127**, pp. 297–305.
[12] Aunapu, N. V., Volino, R. J., Flack, K. A., and Stoddard, R. M., 2000, "Secondary Flow Measurements in a Turbine Passage With Endwall Flow Modification," J. Turbomach., **122**, pp. 651–658.
[13] Ranson, W., Thole, K. A., and Cunha, F., 2005, "Adiabatic Effectiveness Measurements and Predictions of Leakage Flows Along a Blade Endwall," J. Turbomach., **127**, pp. 609–618.
[14] Yamao, H., Aoki, K., Takeishi, K., and Takeda, K., 1987, "An Experimental Study for Endwall Cooling Design of Turbine Vanes," IGTC-1987, Tokyo, Japan.
[15] Piggush, J. D., and Simon, T. W., "Flow Measurements in a First Stage Nozzle Cascade Having Endwall Contouring, Leakage, and Assembly Features," ASME Paper No. GT2005-68340.
[16] Piggush, J. D., and Simon, T. W., 2005, "Flow Measurements in a First Stage Nozzle Cascade Having Leakage and Assembly Features: Effects of Endwall Steps and Leakage on Aerodynamic Losses," ASME Paper No. IMCE2005-83032.
[17] Reid, K., Denton, J., Pullan, G., Curtis, E., and Longley, J., "The Interaction of Turbine Inter-Platform Leakage Flow With the Mainstream Flow," ASME Paper No. GT2005-68151.
[18] Cardwell, N. D., Sundaram, N., and Thole, K. A., 2006, "Effects of Mid-Passage Gap, Endwall Misalignment and Roughness on Endwall Film-Cooling," J. Turbomach., **128**, pp. 62–70.
[19] de la Rosa, Blanco E., Hodson, H. P., and Vazquez, R., "Effect of Upstream Platform Geometry on the Endwall Flows of a Turbine Cascade," ASME Paper No. GT2005-68938.
[20] Radomsky, R., and Thole, K. A., 2002, "Detailed Boundary Layer Measurements on a Turbine Stator Vane at Elevated Freestream Turbulence Levels," J. Turbomach., **124**, pp. 107–118.
[21] "Sandpaper—Coated Abrasives," www.sizes.com/tools/sandpaper.htm (11 August 2004).
[22] Bons, J. P., Taylor, R. P., McClain, S. T., and Rivir, R. B., 2001, "The Many Faces of Turbine Surface Roughness," J. Turbomach., **123**, pp. 739–748.
[23] Modest, M. F., 2003, *Radiative Heat Transfer*, 2nd ed., pp. 743–758.
[24] Ethridge, M. I., Cutbirth, J. M., and Bogard, D. G., 2000, "Scaling of Performance for Varying Density Ratio Coolants on an Airfoil With Strong Curvature and Pressure Gradients," J. Turbomach., **123**, pp. 231–237.
[25] Moffat, R. J., 1988, "Describing the Uncertainties in Experimental Results," Exp. Therm. Fluid Sci., **1**, pp. 3–17.
[26] Kang, M., Kohli, A., and Thole, K. A., 1999, "Heat Transfer and Flowfield Measurements in the Leading Edge Region of a Stator Vane Endwall," J. Turbomach., **121**(3), pp. 558–568.